Light scattering properties of marine particles in coastal and open ocean waters as related to the particle mass concentration

Marcel Babin

Laboratoire d'Océanographie de Villefranche, CNRS/UPMC, B.P. 8, 06238 Villefranche-sur-Mer Cedex, France;
Marine Physical Laboratory, Scripps Institution of Oceanography, University of California at San Diego, La Jolla,
California 92093-0238

André Morel

Laboratoire d'Océanographie de Villefranche, CNRS/UPMC, B.P. 8, 06238 Villefranche-sur-Mer Cedex, France

Vincent Fournier-Sicre

ACRI ST, 260 Route du Pin Montard, B.P. 234, 06904 Sophia Antipolis, France

Frank Fell

Informus GmbH, Gustav-Meyer-Allee 25, 13355 Berlin, Germany

Dariusz Stramski

Marine Physical Laboratory, Scripps Institution of Oceanography, University of California at San Diego, La Jolla,
California 92093-0238

Abstract

   Variations in the spectral scattering coefficient of marine particles [$b_p(\lambda)$] were measured at 241 locations in oceanic (case 1) and coastal (case 2) waters around Europe. The scattering coefficient at 555 nm normalized to the dry mass of particles [$b_p^m(555)$] was, on average, 1.0 and 0.5 m² g⁻¹ in case 1 and case 2 waters, respectively. Spectral variations in $b_p(\lambda)$ were, on average, small in all investigated waters. To understand the observed variations in particle scattering, we performed calculations based on the Mie theory with various values for the slope for the Junge-type size distribution, refractive index, and apparent density of particles (dry weight/wet volume). The latter two were varied according to the type of particles (organic versus mineral) and, for organic ones, as a function of the water content. The higher $b_p^m(555)$ values in case 1 waters are mainly due to the low apparent density, which results from the organic nature of particles and their elevated water content. In all investigated coastal regions, except for the Baltic Sea, the low $b_p^m(555)$ values can be explained by the dominant presence of mineral particles, characterized by a high density that counterbalances the effect of a higher refractive index. In the Baltic Sea, $b_p^m(555)$ was similar to values found in other coastal waters despite the fact that particles were dominantly organic, which may result from higher absorption relative to scattering. A smaller than expected increase of $b_p(\lambda)$ toward short wavelengths is attributed to significant absorption that increases toward the shorter wavelengths and reduces scattering, whether particles are living, detrital, or mineral. Our analyses suggest that the determination of b_p^m may be significantly sensitive to the porosity of the filter used to assess the dry mass of particles.

   Light scattering by suspended particles is generally the first-order determinant of reflectance variability in coastal

waters (so-called case 2, cf. Table 2 title). Consequently, the load of suspended particles would be the quantity estimated with most confidence from reflectance in such waters when measured in the field or from space (Sathyendranath et al. 1989). This statement implies, however, that the ratio of the particle scattering coefficient ($b_p(\lambda)$; m⁻¹) to the dry mass concentration of suspended particles is quantitatively known or predictable with sufficient accuracy. The relationship between $b_p(\lambda)$ and particle load in seawater has been the subject of numerous studies during the 1970s and early 1980s, when various transmissiometers became widely used for studying sediment transport and detecting bottom nepheloid

layers and other hydrodynamical features, as well as for monitoring particulate matter in the open ocean (e.g., Jerlov 1955; Pickard and Giovando 1960; Hunkins et al. 1969; Pak et al. 1970b; Carder and Schlemmer 1973; Baker 1976; Pak and Zaneveld 1977; Kitchen et al. 1978; Zaneveld and Pak 1979; Eggimann et al. 1980; Spinrad and Zaneveld 1982; Baker et al. 1983; McCave 1983).

As theoretically expected, the relationship between $b_p(\lambda)$ and the particle total surface area, or total particle volume concentration (C_v) (*see Table 1* for notation), was shown to change significantly with the particle size distribution and refractive index (e.g., Pak et al. 1970a; Beardsley et al. 1970; Pak et al. 1971; Owen 1974; Carder et al. 1975; Tsuda and Nakata 1982; Spinrad et al. 1983; Baker and Lavelle 1984; Spinrad 1986). The ratio of $b_p(\lambda)$ to the particle total surface area was used to characterize particles in seawater (e.g., Pak et al. 1970a; Carder et al. 1971; Carder and Schlemmer 1973). Note that generally in the above studies, only particles larger than ca. 2 μm were detected using the Coulter counter technique and included in the computation of the particle total surface area.

The relationship between $b_p(\lambda)$ and the more routinely measured dry weight of suspended particulate matter per unit volume of seawater (SPM; g m^{-3}) was also examined. Carder et al. (1975) argued that the mass-specific scattering coefficient, $b_p^m(\lambda) = b_p(\lambda)/\text{SPM}$ (m^2 g^{-1}), would vary less than the ratio of $b_p(\lambda)$ to the particle total surface area because of the more or less concomitant variations in the refractive index (n) and in the "apparent" density of particles (ρ_a). For case 2 waters, the values of b_p^m between 0.1 and 0.8 m^2 g^{-1} were observed in lakes (Hofmann and Dominik 1995), coastal waters (Baker et al. 1983; Baker and Lavelle 1984), and within hydrothermal plumes (Baker et al. 2001). For various open ocean (so-called case 1) waters, a relationship between $b_p(550)$ and SPM was established with an average $b_p^m(550)$ around 1.0 m^2 g^{-1} for the upper layers (Gordon and Morel 1983). Baker and Lavelle (1984) also suggested that a systematic increase in $b_p^m(\lambda)$ would occur from inshore to off-shore waters.

It is not clear whether the range of variation in $b_p^m(\lambda)$, as presently found in the literature, is actual. Over the last decades, many different instruments were used to determine the scattering coefficient of particles (*see* Kirk 1994). Matching the values from the various sensors generally requires assumptions about the scattering phase function of particles. Moreover, SPM has been measured according to various protocols, the main variant being the type and pore size of the filters employed. The filter pore size is critical because small particles, especially those with high refractive index, contribute significantly to scattering (e.g., Tsuda and Nakata 1982, and references therein).

Spectral determinations of $b_p(\lambda)$ have become possible only recently owing to the development of instrumentation for measuring simultaneously the beam attenuation and absorption coefficients (Pegau et al. 1995). Barnard et al. (1998) and Gould et al. (1999) documented spectral variations in $b_p(\lambda)$ in different waters and determined the average $b_p(\lambda)$ spectral shapes with a small standard deviation. These shapes differed from each other, which suggests that they may vary significantly with geographical location. None of

Table 1. Notation.

Para-meter	Value
λ	Light wavelength in vacuum (nm)
a	Total absorption coefficient (m^{-1})
a_w	Pure seawater absorption coefficient (m^{-1})
a_p	Particle absorption coefficient (m^{-1})
a_{NAP}	Absorption coefficient of nonalgal particles (m^{-1})
a_{CDOM}	Absorption coefficient of colored dissolved organic matter (m^{-1})
c	Total beam attenuation coefficient (m^{-1})
b_p	Scattering coefficient of particles (m^{-1})
b_p^m	Mass-specific scattering coefficient of particles (m^2 g^{-1})
$\langle b_p \rangle$	Spectrally averaged scattering coefficient of particles (m^{-1})
Q_a	Efficiency factor for absorption (dimensionless)
Q_b	Efficiency factor for scattering (dimensionless)
N	Number of particles per unit seawater volume per unit size interval (m^{-3} μm^{-1})
D	Particle diameter (μm)
$D_{\min}$	Lower limit of the particle size distribution (μm)
$D_{\max}$	Higher limit of the particle size distribution. (μm)
j	Slope parameter of the Junge-type size distribution, or Junge exponent (dimensionless)
C_v	Particle volume concentration, i.e., the volume of all particles per volume of water sample containing these particles (dimensionless)
ϖ_p	Single scattering albedo (dimensionless)
n	Real part of the refractive index of particles relative to water (dimensionless)
n'	Imaginary part of the refractive index of particles (dimensionless)
n_w	Index of refraction of seawater (dimensionless)
n_o	Index of refraction of dry organic matter (dimensionless)
Δn	Relative increment of refractive index expressed as $(n_o - n_w)/n_w$ (dimensionless)
ρ	Density of particulate matter, i.e., the ratio of wet weight to wet volume of particles ($\times 10^6$ g m^{-3})
ρ_a	Apparent density of particulate matter, i.e., the ratio of dry weight to wet volume of particles ($\times 10^6$ g m^{-3})
ρ_o	Density of dry organic matter ($\times 10^6$ g m^{-3})
ρ_w	Density of pure seawater ($\times 10^6$ g m^{-3})
$\Delta \rho$	Relative density increment expressed as $(\rho_o - \rho_w)/\rho_w$
V_o	Relative partial volume of organic matter in particulate matter (dimensionless)
V_w	Relative partial volume of water in particulate matter (dimensionless)
γ	Exponent of the power law describing the spectral change in $b_p(\lambda)$ for nonabsorbing particles with a Junge-type size distribution (dimensionless)
TChl	Sum of chlorophyll a and phaeopigments concentrations (mg m^{-3})
SPM	Particle dry weight per unit volume of seawater (g m^{-3})
SPM$_{\text{org}}$	Dry weight of total organic matter in seawater (g m^{-3})
SPM$_\phi$	Dry weight of organic matter in seawater associated with phytoplankton (g m^{-3})
S_{NAP}	Spectral slope of the exponential fit applied to the nonalgal particle absorption spectrum (nm^{-1}) (Eq. 14)

Table 2. Dates, locations, and water types of the COASTℓOOC campaigns. The water types are classified as case 1 or case 2 waters (Morel and Prieur 1977) based on historical knowledge of the sites. Case 1 waters are those waters in which phytoplankton, with their associated retinue of material (living or inanimate) of biological origin, are the main agents responsible for variations in optical properties of the water. In contrast, in case 2 waters influenced by terrigenous influx, other substances that vary independently from phytoplankton, notably sediments and dissolved yellow substance, play a major role in governing the optical properties.

COASTℓOOC campaign ID	Sampling platform	Time period	Sampling locations	No. of stations	Water type
1	RV *Victor Hensen*	3–4 Apr 97	North Sea (Rhine river plume) and English Channel	11	Case 2
		4–22 Apr 97	Atlantic; open ocean from Bay of Biscay to Canary Islands	31	Case 1
2	Helicopter	17–19 Jul 97	Lions Gulf: Rhone river plume	3	Case 2
3	Helicopter	21 Jul–2 Aug 97	Northern Adriatic Sea: Po river plume and off the Lido Island	2	Case 2
4	RV *Tethys II*	28 Sep–9 Oct 97	Lions Gulf: Rhone rive plume and surrounding case 1 waters	40	Case 2
6	Helicopter	1–5 Sep 98	English Channel: Tamar, Exe, Dart, Avon, Yealm, Erme, and Fowey river plumes and all along the coast between the Exe and Fal rivers.	45	Case 2
		11–13 Sep 98	North Sea: around Texel Island offshore, in the Marsdiep and in the Wadden Sea	13	Case 2
		16–18 Sep 98	North Sea: between Borkum and Wangerooge Friesland Islands in the Wadden Sea and offshore, and in the Weser river plume.	35	Case 2
		22–25 Sep 98	Baltic: west of Oder river plume between Usedom and Rügen Islands	45	Case 2
Almofront-2 (second leg)	RV *L'Atalante*	25 Dec 97–13 Jan 98	Alboran Sea	11	Case 1, as identified by Morel and Maritorena (2001)
Total				241	

these studies examined specifically the causes of variability in the $b_p(\lambda)$ spectrum.

In this study, we present results from an intensive sampling program conducted in European coastal and open ocean waters, where $b_p(\lambda)$ and $b_p^m(\lambda)$ were always determined using the same protocol. For the same waters, Babin et al. (in press) analyzed the variations in the absorption coefficient of phytoplankton, nonalgal particles, and colored dissolved organic matter. Here our objectives are (1) to determine the variability in magnitude and spectral behavior of $b_p^m(\lambda)$ for a variety of water types and (2) to understand the causes of the observed variability based on theoretical considerations and some knowledge of the chemical composition of particles. This study was prompted by the recent availability of commercial in situ sensors that allow determinations of $b_p(\lambda)$ over the visible spectrum. Additionally, new ocean color sensors with improved capabilities for optical remote sensing in coastal waters are becoming operational (e.g., the MODIS and MERIS sensors). These new tools provide potentially powerful means for monitoring the sediment load in coastal waters at various space and time scales. The quantitative use of these tools is currently limited by our incomplete understanding of the scattering properties of marine particles, in particular because of the diversity in their chemical nature.

Sampling and methods

Sampling was conducted in various coastal waters around Europe during six campaigns in 1997 and 1998, as part of the COASTℓOOC (coastal surveillance through observation of ocean color) research project. More than 15 river plumes, other coastal environments (e.g., Wadden Sea), and zones where sediment resuspension occurs were surveyed in the Mediterranean Sea, Baltic Sea, North Sea, and English Channel (Table 2). Additionally, case 1 water samples were collected in the northeast Atlantic Ocean between the Biscay Bay and the Canary Islands off the continental shelf (beyond the 200-m isobath), and in the Alboran Sea during the second leg of the Almofront-2 cruise (Fig. 1) (*see* Claustre et al. 2000 for a detailed description of the latter cruise).

At 241 stations, the spectral absorption, $a(\lambda)$, and beam attenuation, $c(\lambda)$, coefficients were measured in the surface layer using an ac-9 profiler (WET Labs) deployed either from a ship or from a helicopter. The instrument included the following spectral bands (bandwidth of ca. 10 nm): 412, 440, 488, 510, 555, 630, 650, 676, and 715 nm. Profiles of $a(\lambda)$ and $c(\lambda)$ were recorded with ca. 10-cm vertical resolution (6 Hz sampling rate at ca. 0.5 m s^{-1} falling speed of the instrument), from surface down to the bottom, or down to at least 40 m, when allowed by bathymetry. The manu-
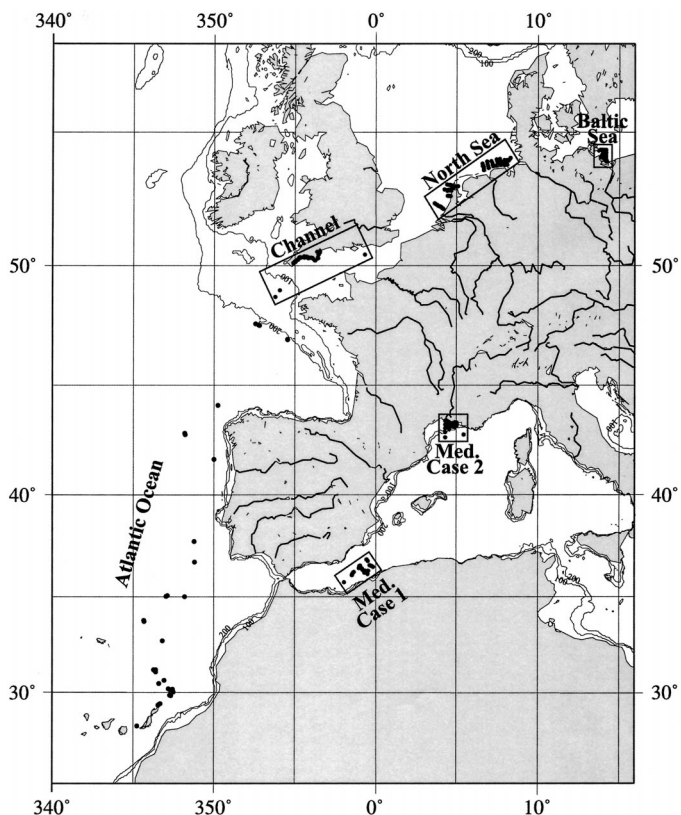
Fig. 1. Location of 241 stations visited during the COASTℓOOC study and the Almofront-2 cruise. The partitioning into regions are all shown within rectangles, except those in the Atlantic Ocean. The 100- and 200-m isobaths are displayed.

facturer calibration was checked daily using pure water. Correction for change in pure water absorption and attenuation due to temperature and salinity was made according to Pegau et al. (1997). Correction of absorption for scattering error was achieved by subtracting $a(715)$ from $a(\lambda)$ (Zaneveld et al. 1994). In this study, the mean $a(\lambda)$ and $c(\lambda)$ spectra were calculated for each station by averaging data collected within the first attenuation depth when this layer was vertically homogenous, or within the first 2 m when it was stratified. Because the ac-9 profiler is calibrated with pure water as reference, the $a(\lambda)$ and $c(\lambda)$ output values exclude the contribution of pure water [$a_w(\lambda)$ and $c_w(\lambda)$]. The particle scattering coefficient, $b_p(\lambda)$, is then obtained directly from $c(\lambda) - a(\lambda)$. In the North Sea and Baltic Sea (COASTℓOOC 6 cruise) an additional ac-9 was generally used with a 0.2-μm filter (Gelman Suporcap) mounted on the inlet of the reflective tube in order to also measure the absorption coefficient of colored dissolved organic matter [$a_{CDOM}(\lambda)$].

At all stations, a water sample (6-liter polyethylene or 8-liter Niskin bottle) was collected just below surface for in vitro analyses. On board the ship, water samples were analyzed and/or stored immediately after collection. When using a helicopter as sampling platform, water samples were kept in 6-liter polyethylene containers no longer than 2 h after sampling. Filtration was conducted at low vacuum onto 25-mm glass fiber filters (Whatman, GF/F) to collect particles

for subsequent analyses, as described below. Because of the texture of these filters, their pore size is not sharply defined. A nominal value often used is 0.7 μm, but the effective pore size seems to be substantially smaller (Sheldon 1972). It was shown, for instance, that tiny organisms such as prochlorophytes (diameter slightly above 0.5 μm) are quantitatively retained on GF/F filters (Chavez et al. 1995).

Four separate subsamples (up to 2 liters each) were filtered for each sample with the following purposes.

(i) The absorption spectrum of particles retained onto a GF/F filter, $a_p(\lambda)$, was measured using the transmittance–reflectance (*T-R*) technique (Tassan and Ferrari 1995) as described by Babin et al. (in press). Briefly, the particles collected on a GF/F filter were kept in liquid nitrogen for up to 2 months before analysis in the laboratory. Absorbance and reflectance were measured between 380 and 750 nm with a 1-nm increment using a dual beam spectrophotometer equipped with a 60-mm integrating sphere.

(ii) To determine the concentration of suspended particulate matter (SPM; g m^{-3}), the particles collected onto a pre-weighed GF/F filter were dried and stored in a freezer at $-80°$C until the dry weight was determined less than 2 months later in the laboratory (van der Linde 1998).

(iii) For pigment analysis, the filter with collected particles was inserted into a cryotube and kept in liquid nitrogen until analysis less than 3 months later. High-performance liquid chromatography (HPLC) was used as described by Vidussi et al. (1996) to determine liposoluble pigment concentrations. TChl is here defined as the sum of chlorophyll *a*, divinyl-chlorophyll *a*, chlorophyll *a* isomer and epimer, chlorophyllids *a*, and phaeopigments.

(iv) The concentration of particulate organic carbon (*POC*) was determined using a Carlo Erba NCS 2500 elemental analyzer as described in Ferrari et al. (in press). These determinations were made on particles collected onto a GF/F filter precombusted at 450°C for 2 h and stored in the freezer at $-80°$C until analysis less than 2 months later.

The contribution of organic matter to SPM can be estimated as follows. The first approach is based on a relationship between the dry mass of organic matter, SPM$_{org}$, and the particulate organic carbon content. The average relationship, corresponding to the mean organic matter composition, is (Copin-Montégut 1980; van Raaphorst and Melschaert 1996)

$$SPM_{org}/POC = 2.6 \text{ g g}^{-1} \qquad (1)$$

By using this ratio, the POC values can be converted into SPM$_{org}$, and then the SPM$_{org}$/SPM ratio can be assessed (Table 3). SPM$_{org}$ will be referred to as the total suspended organic matter, and we will assume that the difference SPM $-$ SPM$_{org}$ represents mineral particles. A different approach can be employed to derive another quantity characterizing the organic matter, SPM$_{\phi}$, namely, the dry mass of organic matter associated with the presence of phytoplankton plus covarying materials (living and inanimate particles). An empirical relationship, dealing exclusively with case 1 waters, has been established (Morel 1988):

$$POC = 90(TChl)^{0.57} \qquad (2)$$

It is assumed that POC represents only the particulate carbon

Table 3. Regional averages of SPM, TChl, and the mass ratio of organic to dry particulate matter (SPM_{org}:SPM). SPM_ϕ:SPM was calculated as described in the text. Normality of distributions was verified successfully using a Komolgorov-Smirnov test on log-transformed data. The geometric standard deviation (SD) is shown in italic below the average (to be applied as a factor). The average SPM_{org}:SPM values were compared between investigated regions using a Fisher PLSD test. These values were considered significantly different when $p < 0.0001$. The column "Different from regions" shows the regions identified through ID, which are significantly different from a given region listed in the column "Region." Note that only samples for which scattering data were available are considered. No. is the number of observations.

ID	Region	SPM (g m⁻³) No.	SPM (g m⁻³) Average SD	TChl (mg m⁻³) No.	TChl (mg m⁻³) Average SD	SPM_ϕ:SPM (%)	SPM_{org}:SPM (%) No.	SPM_{org}:SPM (%) Average SD	Different from regions (ID)
a	Atlantic	29	0.083 *2.2*	27	0.16 *2.2*	99	8	93 *1.8*	d, e, f
b	Med. case 1	—	— *—*	15	0.75 *1.3*	—	—	— *—*	—
c	Baltic	44	2.3 *1.7*	43	9.3 *1.8*	36.3	21	87 *1.4*	d, e, f
d	Channel	48	0.84 *1.7*	42	0.89 *1.7*	26.1	45	36 *1.6*	a, c, e, f
e	Med. case 2	43	1.0 *3.2*	36	0.57 *3.6*	17	40	20 *2.1*	a, c, d
f	North Sea	56	6.56 *2.4*	49	11.7 *2.2*	12.8	51	17 *1.7*	a, c, d

content of phytoplankton and their covarying materials, as the above relationship is valid for waters far from land influence. The POC values estimated from the chlorophyll concentration (via Eq. 2) are then transformed into SPM_ϕ by again using Eq. 1. The quantities SPM_ϕ and SPM_{org} may differ to the extent that allochthonous organic matter (brought by rivers, for instance) adds to SPM_{org}, not to SPM_ϕ. Therefore, SPM_ϕ and SPM_{org} normalized to SPM can be compared to detect the presence of allochthonous organic particles (Table 3).

From the determinations described above, it is possible to derive $\varpi_p(\lambda)$, the single-scattering albedo of marine particles, defined as

$$\varpi_p(\lambda) = \frac{b_p(\lambda)}{a_p(\lambda) + b_p(\lambda)} \quad (3)$$

which is a fundamental parameter in radiative transfer and light scattering models. The $a_p(\lambda)$ coefficients, determined via the T-R technique, ignore the tiny particles that have passed through the GF/F filter (Stramski 1990), while the $b_p(\lambda)$ coefficients, determined in situ, account for their presence. This difference may affect (overestimate) the $\varpi_p(\lambda)$ values. Fortunately, the in situ measurements of $a_{CDOM}(\lambda)$ made with an ac-9 at 80 stations in the North Sea and Baltic Sea allow $a_p(\lambda)$ for all particles to be derived as

$$a_p(\lambda) = a(\lambda) - a_{CDOM}(\lambda) \quad (4)$$

For these stations, $\varpi_p(\lambda)$ can be computed using $a_p(\lambda)$ values determined by the two different methods. The relative difference in terms of the derived $\varpi_p(\lambda)$ values was always less than 5%, which means that the suspected difference is insignificant.

Experimental results

Load and nature of particles—In the data analyzed here, the SPM values encompassed about three orders of magnitude (0.019 to 72.8 g m⁻³) and TChl about two orders of magnitude (0.055 to 40.2 mg m⁻³). The smallest SPM and TChl values were observed in case 1 Atlantic waters, and the largest values in the North Sea, followed by those in the Baltic Sea.

From the TChl values, the estimated SPM_ϕ were on average 0.082, 0.834, 0.219, 0.170, and 0.841 g m⁻³ in the Atlantic Ocean, Baltic Sea, English Channel, Mediterranean Sea, and North Sea, respectively. The average ratios SPM_ϕ: SPM and SPM_{org}:SPM are listed in Table 3 for the different regions. Some interesting features emerge from the comparative examination of these two ratios. First of all, they are ordered in the same way from region to region, which shows the consistency of the three independent data sets (SPM, POC, and TChl). These data demonstrate that the particulate material in the Atlantic case 1 waters is essentially organic and related to the algal population (with $SPM_\phi \approx SPM_{org}$). The ratios also show that organic matter in the investigated case 2 waters represents a widely varying fraction of the suspended particulate material, from 87 to 17% (or 36 to 13% in terms of algae-related matter). Even when the mineral fraction is dominating [e.g., $(SPM - SPM_{org})/SPM = 83\%$ in the North Sea, or 80% in Mediterranean case 2 waters], the algal fraction is never negligible. The Baltic waters are clearly different, with the highest relative algal content (SPM_ϕ:SPM = 36% and a mean TChl value of 9 mg m⁻³), an extremely high proportion of organic matter (SPM_{org}: SPM = 87%), and consequently the lowest (13%) mineral content found for case 2 waters.

Relationship between $b_p(\lambda)$ and SPM, and spectral dependency of $b_p(\lambda)$—The wavelength 555 nm (corresponding to
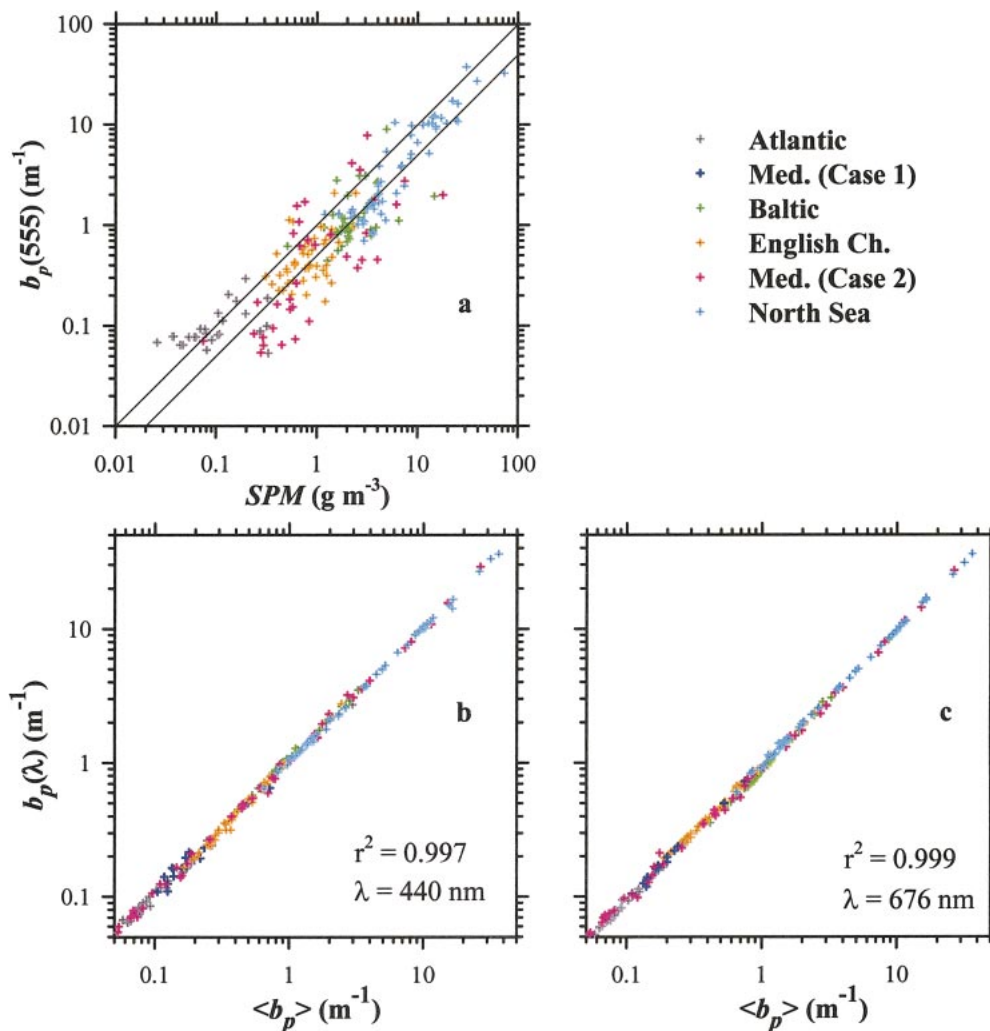
Fig. 2. Scatter plot of (a) $b_p(555)$ as a function of SPM (the 1:1 and 1:2 lines are shown), (b) $b_p(440)$ as a function of $\langle b_p \rangle$, and (c) $b_p(676)$ as a function of $\langle b_p \rangle$.

a minimal absorption by particulate matter) is selected for an overall examination of the relationship between scattering and particle mass concentration. The $b_p(555)$ values are plotted versus SPM for all geographic regions in Fig. 2a, and mean values of the mass-specific scattering $b_p^m(555)$ are provided in Table 4 for each region.

The data in Fig. 2a are scattered. This is partly due to region-to-region differences, natural variability in $b_p^m(555)$ within any given region, and also due to experimental random error. In practice, the in situ optical determinations of $b_p(\lambda)$ and water sampling for SPM analysis cannot perfectly coincide in time and space. In spite of the care taken to reduce the delay between the two operations, the internal compatibility of the two measurements might remain questionable, particularly in patchy case 2 waters. Nonetheless, the general trend in the $b_p(555)$ versus SPM relationship is well captured, and the region-by-region analysis reveals significant results (Table 4). The Atlantic case 1 waters are clearly different, with the highest $b_p^m(555)$ value of about 1.0 m² g⁻¹. In contrast, all the case 2 waters, with roughly sim-

ilar mean values, exhibit $b_p^m(555)$ values close to 0.5 m² g⁻¹, i.e., half of that typical of case 1 waters.

To put in evidence the varying shape of the scattering spectrum, the $b_p(\lambda)$ values are normalized with respect to the spectrally averaged scattering coefficient, $\langle b_p \rangle$, computed between the extreme spectral bands as

$$\langle b_p \rangle = \left(\frac{1}{303} \right) \int_{412}^{715} b_p(\lambda)\, d\lambda \qquad (5)$$

In this way, there is no preferential wavelength in the statistical analysis. Figures 2b and 2c show examples of the variations of $b_p(\lambda)$ with $\langle b_p \rangle$, both plotted on logarithmic scales. Similar plots using $b_p(555)$ instead of $\langle b_p \rangle$ lead to similarly high correlation coefficients (*see Table 5*). The slopes (~1) and negligible intercept values result in an approximately 1:1 linear relationships between $b_p(\lambda)$ and $\langle b_p \rangle$. A closer examination shows, however, that these relationships actually differ from one region to another, and the average spectral values of the ratios $b_p(\lambda):\langle b_p \rangle$ are displayed for each region in Fig. 3a.
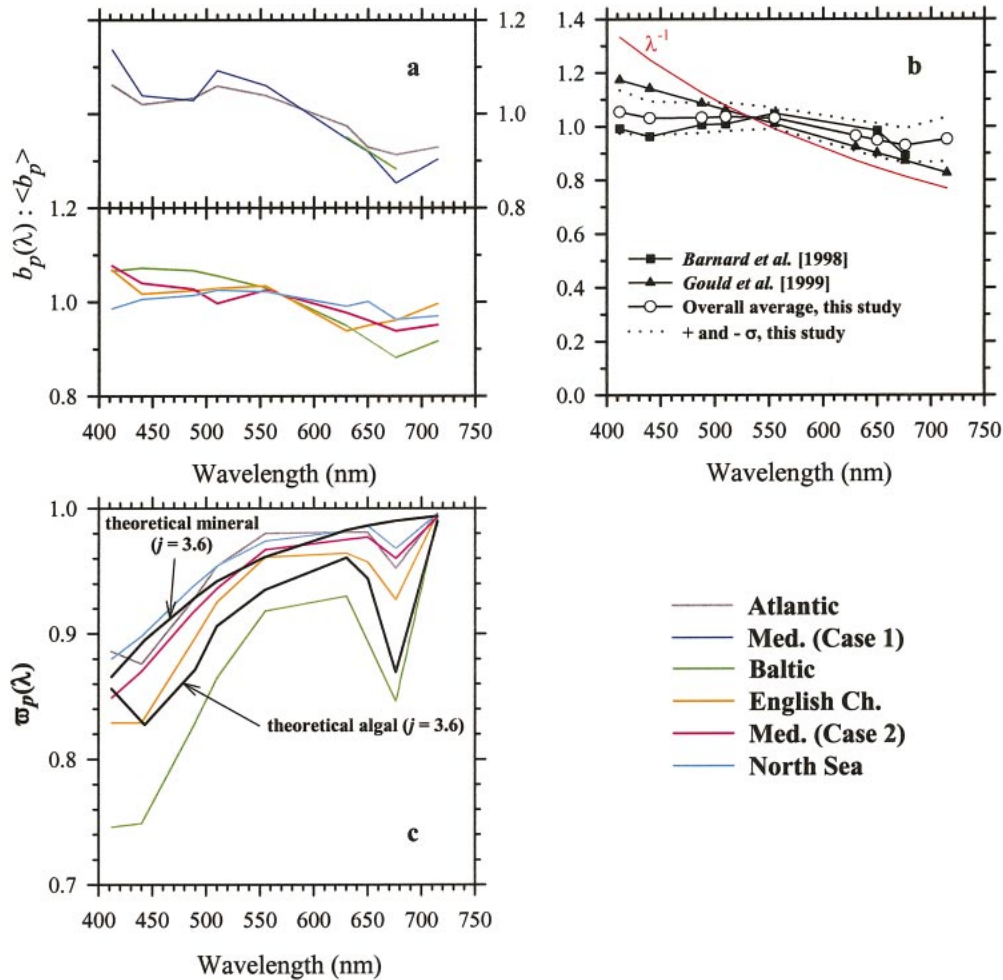
Fig. 3. Average spectra of the $b_p(\lambda):\langle b_p \rangle$ ratio; (a) separately for the different regions and (b) for all samples. Note that no data were available at 650 nm for the North Sea and Baltic Sea during cruise 6. The λ^{-1} dependency and the average spectra of Barnard et al. (1998) and Gould et al. (1999) are also shown in (b), together with the standard deviation for all our samples. (c) Average spectra of the single-scattering albedo of particles for the different regions and theoretical spectra for typical pure algal and pure <u>mineral</u> particles (*see text for details*). Average spectra were determined on data transformed as $\sqrt{1-x}$ to obtain normality and are presented after a back transformation $(1-y^2)$.

The trough in the scattering spectra around 676 nm corresponding to the red absorption of chlorophyll *a* is present in all curves in a more or less pronounced fashion. A minimum around 440 nm, also a print of algal absorption on scattering, is less systematic. Both these minima are found in case 1 waters (Atlantic and Mediterranean) (upper panel in Fig. 3a). In contrast, in case 2 waters, the spectra are flatter and less structured (lower panel). For the Baltic Sea, the ascending slope toward the shorter wavelengths is the steepest one, and the convexity of the curve in the blue part of the spectrum is noticeable (also in the North Sea). Regardless of the water type and regions, all the spectra practically coincide near 550–600 nm, likely as a result of a smaller influence of absorption on scattering in this spectral domain.

Despite the notable differences among the various spectra,

a mean spectrum for all data has been computed, essentially with the purpose of comparing with other published spectra (Fig. 3b). A λ^{-1} dependency is steeper than our mean spectrum and inconsistent with the present dataset. The linear relationship between $b_p(\lambda)$ and λ, which results from observations by Gould et al. (1999) in both case 1 and case 2 waters, is also steeper. The mean spectrum derived by Barnard et al. (1998) from their observations in various waters, including case 2, remains within 1 SD from the present mean spectrum. The effect of algal pigments is more pronounced in the Barnard et al. spectrum compared to the present mean spectrum.

Relative variations in the absorption and scattering coefficients of particles—The spectral values of the single-scattering albedo, $\varpi_p(\lambda)$, averaged for each region separately,

Table 4. Overall and site-by-site statistics of the $b_p(555)$:SPM ratio. Normality of distributions was verified successfully using a Komolgorov–Smirnov test on log-transformed data. The geometric standard deviation (SD) is to be applied as a factor. Averages were compared between regions using a Fisher PLSD test. They were considered as significantly different when $p < 0.0005$. The column "Different from regions (ID)" shows the regions identified through ID, which are significantly different from a given region listed in the region column. No SPM data were collected in Med. (case 1). Note that only samples for which scattering data were available are considered. No. is the number of observations.

ID	Region	No.	Average ($m^2\ g^{-1}$)	SD	Different from regions (ID) ($p < 0.0005$)
a	Atlantic	25	0.97	1.9	c, d, e, f
b	Med. (case 1)	—	—	—	—
c	Baltic	44	0.49	1.7	a
d	Channel	46	0.56	1.7	a
e	Med. (case 2)	35	0.42	2.6	a
f	North sea	55	0.54	1.6	a
—	All case 2	180	0.51	1.9	—

are shown in Fig. 3c. All spectra exhibit a general decrease from 715 nm (where ϖ_p is essentially 1) toward short wavelengths and have a secondary minimum at 676 nm associated with the red absorption peak of chlorophyll (and phaeopigments). The knee at 443 nm, associated with the blue absorption by pigments (chlorophylls and carotenoids), is distinctly marked in case 1 waters (Atlantic) and smoother in case 2 waters, or even absent (North Sea and Mediterranean case 2 waters) when the phytoplankton contribution is minimal (*see* Table 3). The Baltic Sea values are noticeably below those from other regions. Not only the minimum at 676 nm is deeper, but also the ϖ_p values in the blue part of the spectrum are distinctly lower, which reveals that particles in the Baltic are more "colored," i.e. more absorbing in the blue domain (recall that they are mainly organic, Table 3).

Theoretical background

In this section, the theoretical basis for interpretation of the particle scattering properties is presented. Some of these considerations, which can be found in the literature, are here revisited and reassembled, before being used when interpreting our field observations (next section).

Mass-specific and volume-specific scattering coefficient— To the extent that the size distribution and the chemical nature of particles are known, the corresponding scattering coefficient can be predicted, at least under simplifying assumptions. The main assumption is that irregularly shaped and randomly oriented particles scatter light like spherical particles with some equivalent diameter D. Additionally, all the particles are assumed to be homogeneous, and all have the same refractive index relative to water, $m = n - in'$, where n is the real part of the refractive index and n' the imaginary part. Under these assumptions, Mie theory can be used to compute the efficiency factors for scattering, $Q_b(\lambda)$, and for absorption, $Q_a(\lambda)$, of individual particles with any diameter D and any refractive index. The refractive index depends on the chemical composition of the particles, which in turn determines the particle density needed to derive the scattering coefficient per unit mass concentration, $b_p^m(\lambda)$. Thus, for a population of particles having the same refractive index and density we can write (*see* Spinrad 1986):

$$b_p(\lambda) = \left(\frac{\pi}{4}\right) \int_{D_{max}}^{D_{min}} N(D)Q_b(\lambda,\ D)D^2\ dD \qquad (6)$$

$$C_v = \left(\frac{\pi}{6}\right) \int_{D_{min}}^{D_{max}} N(D)D^3\ dD \qquad (7)$$

$$b_p^m(\lambda) = \frac{b_p(\lambda)}{SPM} = \frac{b_p(\lambda)}{(C_v\rho_a)} \qquad (8)$$

where $N(D)dD$ is the number of particles in the size interval from D to $D + dD$ per unit water volume, C_v (dimensionless)

Table 5. Overall and site-by-site statistics for the ratio $b_p(\lambda):b_p(555)$ at different wavelengths (as indicated by the column headers). For each site and wavelength, the average is provided with the corresponding arithmetic standard deviation underneath (in italic). No. is the number of observations. Note that no data were available at 650 nm for the North and Baltic Sea during cruise 6.

Region	No.	412:555	440:555	488:555	510:555	630:555	650:555	676:555	715:555
Atlantic	31	1.024	0.984	0.996	1.021	0.939	0.896	0.881	0.894
		0.102	*0.090*	*0.055*	*0.056*	*0.067*	*0.073*	*0.057*	*0.037*
Med. (case 1)	16	1.072	0.980	0.970	1.030	0.896	0.871	0.808	0.858
		0.097	*0.099*	*0.087*	*0.084*	*0.144*	*0.136*	*0.124*	*0.217*
Baltic	45	1.036	1.041	1.036	1.026	0.922	—	0.857	0.891
		0.059	*0.046*	*0.041*	*0.042*	*0.040*		*0.055*	*0.059*
Channel	48	1.035	0.985	0.992	0.996	0.907	0.920	0.930	0.964
		0.089	*0.074*	*0.060*	*0.038*	*0.032*	*0.039*	*0.042*	*0.061*
Med. (case 2)	43	1.056	1.019	1.007	0.976	0.955	0.941	0.919	0.931
		0.129	*0.105*	*0.108*	*0.076*	*0.065*	*0.083*	*0.103*	*0.100*
North Sea	56	0.966	0.985	0.993	1.003	0.970	1.020	0.943	0.950
		0.054	*0.047*	*0.034*	*0.019*	*0.027*	*0.048*	*0.044*	*0.041*
All	239	1.025	1.003	1.003	1.005	0.937	0.922	0.904	0.925
		0.095	*0.080*	*0.068*	*0.054*	*0.063*	*0.083*	*0.081*	*0.089*

is the particle volume concentration, and ρ_a is the apparent density of particles (*see Table 1*). The above integrals are calculated between the limits D_{min} and D_{max}, which represent the minimal and maximal sizes considered (discussed below). The number size distribution is often assumed to follow the Junge distribution:

$$N(D) = KD^{-j} \tag{9}$$

where K sets the scale and j is the slope of the distribution. Typical values of j for most of the marine particle populations vary within the range 3–5, although we must note that the most data are available for particles larger than 1–2 μm (e.g., Bader 1970; Sheldon et al. 1972).

The simplicity of the above equations actually conceals a numerical pitfall, as well as a question about the significance of such computations. The integral expressed by Eq. 6 converges and produces a finite value for $b_p(\lambda)$ when the limits D_{min} and D_{max} are 0 and ∞, provided that $3 < j < 7$ (*see* Morel 1973). This result comes from the fact that $Q_b(\lambda)$ varies as D^4 for extremely small particles (belonging to the Rayleigh scattering domain) and that $Q_b(\lambda)$ becomes constant for optically large particles. With j around 4, and when D_{min} and D_{max} are set equal to 0.02 and 200 μm, respectively, the integral (Eq. 6) captures almost entirely the quantity $b_p(\lambda)$ (Fig. 4a, and *see also* Morel and Ahn 1991 and Stramski and Kiefer 1991). It is worth remarking that if 1.18 and 1.05 are considered as representative n values for mineral and algal particles respectively (e.g., Aas 1996), about half of the scattering is due to particles smaller than 1 μm when they are mineral, whereas the most efficient particles in building the scattering coefficient of algae are in the range 1–10 μm (Fig. 4a).

With regard to the particle volume concentration, it is easy to notice that the integral (Eq. 7) is never finite. This integral depends on either D_{min} or D_{max}, according to the value given to the exponent j (Fig. 4b). If $j = 4$ (or higher), C_v tends toward infinity when D_{min} tends toward 0. In other words, C_v continues to increase when D_{min} decreases. The contrary holds true when $j < 4$. In this case, the relative contribution of the small-sized fraction to the total particle volume decreases, so that the choice of D_{min} becomes less crucial, but the volume continues to increase when the upper limit D_{max} is increasing. This second situation ($j < 4$) is relatively more completely defined than the preceding one because the value of D_{max} is easier to select (large particles are more easily detected and counted than submicron particles). When $j \geq 4$, the choice of D_{min} becomes crucial as it affects the resulting C_v value. The difficulty is that the tiny particles in the colloid size range are generally not measured or enumerated with existing techniques for particle sizing and counting. Therefore, the shape of the distribution in this size range is generally unknown, and the lower limit of the integral D_{min} is somewhat arbitrary.

In an initial series of computations using Mie theory, the particles were assumed to be nonabsorbing ($n' = 0$) at the wavelength considered, 555 nm, and the real part of the index of refraction was varied from 1.01 to 1.21. This range encompasses the biogenic material (1.02–1.08) and the minerogenic particles (1.15–1.20, *see Table 6*). The j exponent was given values between 3.2 and 4.8. The limits D_{max} and
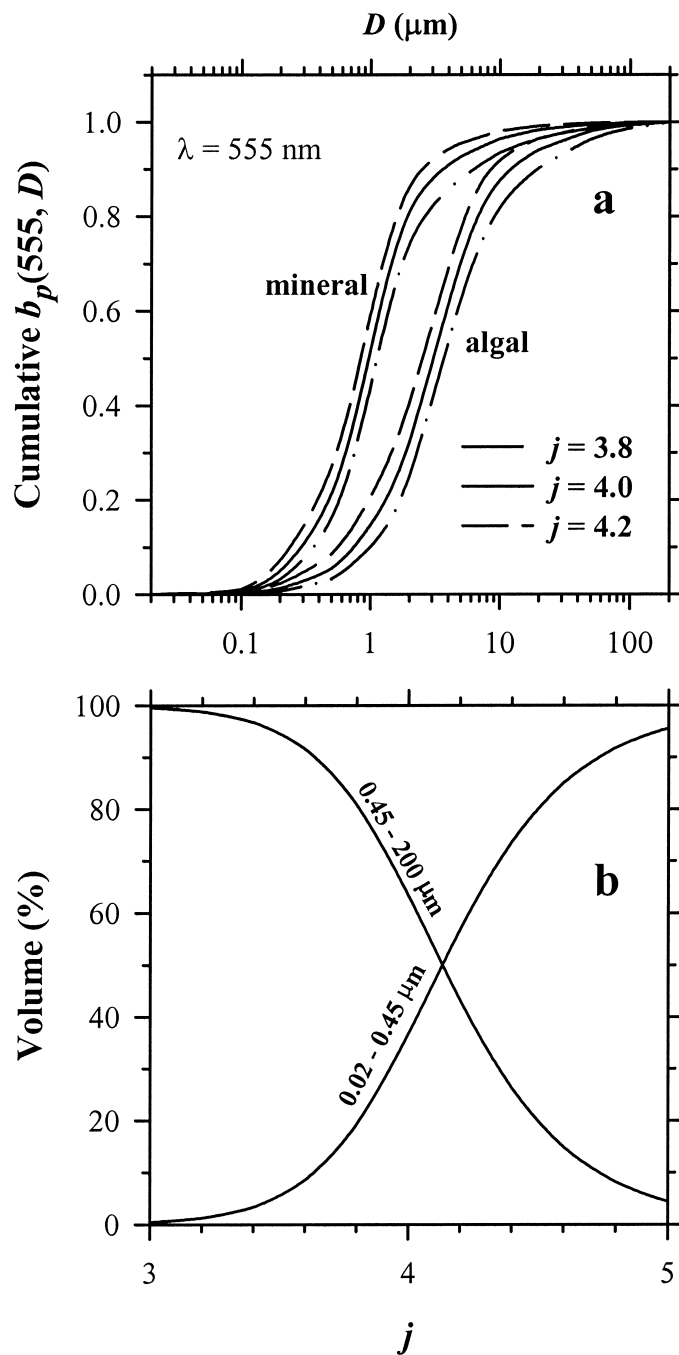

Fig. 4. (a) Theoretical relationship between the cumulative $b_p(D)$ at $\lambda = 555$ nm and particle diameter (D) for typical mineral and algal particles and for different slopes of the size distribution (*see text for details*). (b) Calculated volume of particles with diameter between 0.02 and 0.45 μm and between 0.45 and 200 μm, relative to the sum of these two fractions, plotted as a function of the slope of a Junge-type particle size distribution (j).

D_{min} were given values of 200 and 0.02 μm, respectively. The choice for D_{min} is based on the fact that in situ optical measurements are not intrusive and thus leave unmodified size distributions that include viruses and small debris. When computing C_v, however, D_{min} is set equal to 0.45 μm because

Table 6. Properties of typical particle types found in coastal waters. Density and real part of the refractive index are from Lide (2001). The refractive index n was calculated relative to water by assuming $n_w = 1.34$. The listed refractive index values are the averages over the two or three coordinate axes of the molecular structures. The b_p^m values ($m^2\ g^{-1}$) were obtained at 550 nm from Mie calculations and Eqs. 3–5 assuming $n' = 0$, and j values as indicated.

| Particle type	Density ($\times 10^6$ g m^{-3})	Relative refractive index	b_p^m $j = 3.6$	$j = 3.8$	$j = 4.0$
Aragonite	2.83	1.22	0.26	0.41	0.63
Calcite	2.71	1.17	0.24	0.37	0.54
Chlorite	2.5	1.21	0.29	0.45	0.68
Gibbsite	2.42	1.18	0.27	0.41	0.60
Illite	2.8	1.18	0.23	0.35	0.52
Kaolinite	2.65	1.16	0.23	0.36	0.52
Montmorillonite	2.5	1.17	0.25	0.38	0.55
Opal	1.9	1.07	0.19	0.25	0.32
Quartz	2.65	1.16	0.22	0.34	0.49
Organic matter (dry)	1.38	1.16	0.43	0.65	0.94
Living organic matter (+ water)	0.2–0.5	1.03–1.05	0.77	0.89	0.99

Fig. 5. Theoretical relationship between the $b_p(555):C_v$ ratio and the relative refractive index of particles for different slopes (j) of the particle size distribution.

smaller particles are not retained through filtration on GF/F filters.

The results of these computations are displayed in Fig. 5, where the quantity $b_p(\lambda)/C_v$ (the volume-specific scattering coefficient) is plotted as a function of the relative index of refraction for several j values. Once divided by the appropriate ρ_a value, the corresponding $b_p^m(\lambda)$ values are straightforwardly derived (Eq. 8). Note that the values displayed in Fig. 5 appreciably differ from those in the diagram presented by Spinrad (1986, his fig. 1). This is because the size range (1–80 μm) in Spinrad's study was kept unchanged when computing $b_p(\lambda)$ and C_v and differed from the size ranges considered here. In addition, Spinrad's computations were based on the approximation of van De Hulst (1957), which becomes invalid when the index of refraction departs significantly from 1, as is the case for mineral particles.

As expected, the quantity $b_p(\lambda)/C_v$ regularly increases with n, and for a given n increases strongly with the j value. This increase partly originates from the differing lower limits D_{min} in the calculations of $b_p(\lambda)$ and C_v. By using Eq. 7, it is easy to compute the contributions of small particles (size between 0.02 and 0.45 μm) and larger particles (0.45–200 μm) to the total particle volume C_v associated with the size range 0.02–200 μm (Fig. 4b). When j is about three, C_v essentially results from particles >0.45 μm, so that dividing $b_p(\lambda)$ by C_v is meaningful. Conversely, when j approaches five, more than 95% of the volume is confined within the small-sized fraction, and the quantity $b_p(\lambda)/C_v$ becomes extremely high and meaningless. This disproportionately large contribution of the smallest particles obviously casts doubt on the validity of extrapolating such steep Junge distributions ($j > 4$) toward the small-sized particles. The increase in $b_p(\lambda)/C_v$ for increasingly high j values in Fig. 5 is thus mostly due to the division by a progressively diminishing C_v quantity.
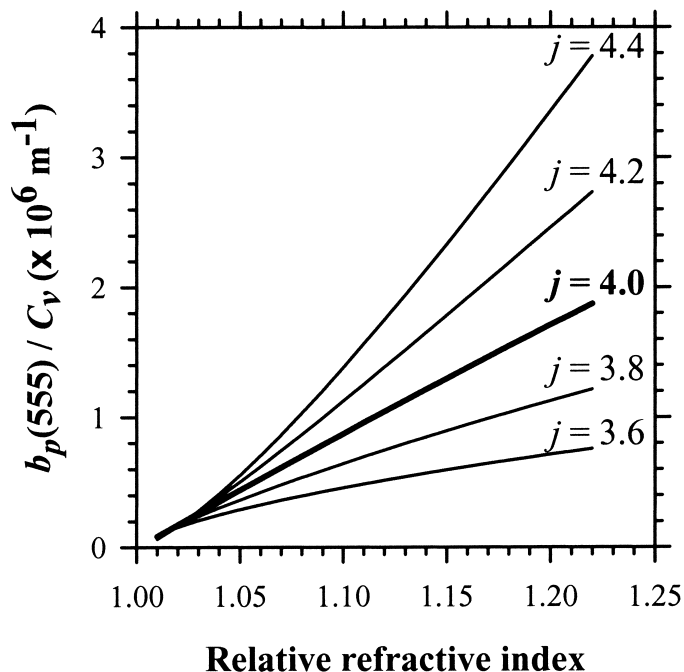
Organic particles—Organic particles may be living (viruses, bacteria, phytoplanktonic cells, heterotrophic plankton) or nonliving bodies (debris, colloids). They are assumed to be essentially made of organic compounds (major metabolites are proteins, carbohydrates, and lipids) plus water. The occurrence of biogenic inorganic material (calcite and silica) forming exoskeleton, or broken detached scales, will be examined separately, together with mineral particles.

Following the approach of Morel and Ahn (1990), and based on the same values of density and refractive index for organic matter (adopted from Aas 1981, *see also* Aas 1996), a prediction of $b_p(\lambda)$ for this particulate material is possible. The partial water volume and the partial dry organic matter volume are denoted V_w and V_o, respectively, with $V_w + V_o = 1$. The refractive index of a "mixture" of these components forming the organic particulate matter relative to water, n, is obtained according to a mixing rule:

$$n = (n_w V_w + n_o V_o)/n_w$$

where n_w and n_o are the refractive indices of water and dry organic matter, respectively. This equation can be rewritten as

$$n = 1 + \Delta n V_o \qquad (10)$$

where Δn is the relative increment of index, expressed as ($n_o - n_w)/n_w$. This increment is, on average, 0.158 and is rather insensitive to the metabolite composition (Morel and Ahn 1990).

In the same way, the relative (to water) density of the watery material forming the mass of a particle is

$$\rho = \rho_m/\rho_w = 1 + \Delta\rho V_o \qquad (11)$$

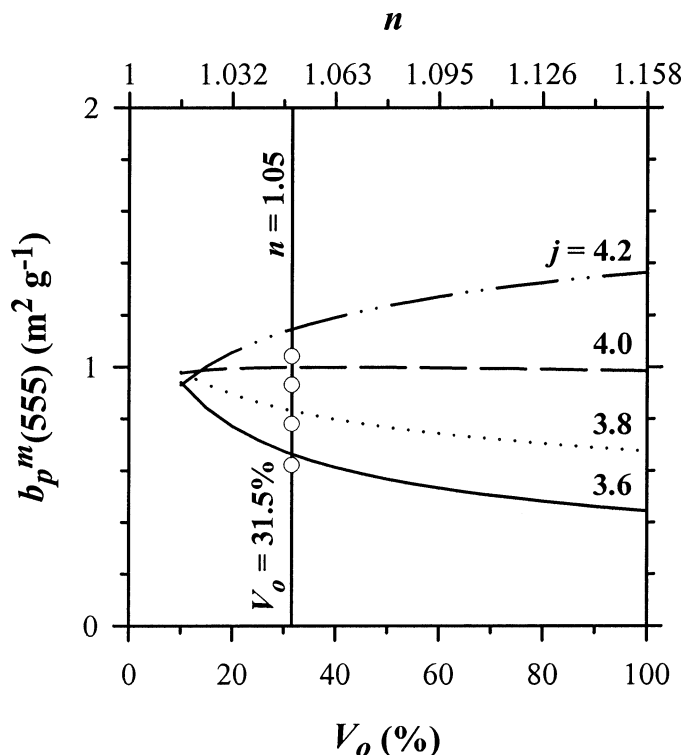where $\Delta\rho$ is the relative density increment expressed as (ρ_o

Fig. 6.   Theoretical changes in $b_p^m(555)$ as a function of the partial volume of organic matter in algal cells (percent V_o) and the relative index of refraction (n) of whole cells, for four different slopes of the Junge-type size distribution. The vertical solid line indicates a typical n value for phytoplankton and the corresponding V_o. The open circles show the $b_p^m(555)$ decrease induced by a change in n' from 0 to 0.0007.

Fig. 7.   The index of refraction relative to seawater for various minerals as a function of particle density. The n and ρ values (also listed in Table 6) are from Lide (2001). The n values are the arithmetic average of the values given for the two or three structure coordinate axes. The plotted minerals are aragonite (A), calcite (Ca), chlorite (Ch), gibbsite (G), illite (I), kaolinite (K), montmorillonite (M), opal (Op), and quartz (Q). The theoretical relationship between n and ρ is also shown for organic matter (*see text for details*).

$- \rho_w)/\rho_w$. This increment is 0.352 when ρ_o, the density of the (dry) organic matter, is given the mean value 1.384×10^6 g m^{-3} (Morel and Ahn 1990) and the density of water is $\rho_w = 1.024 \times 10^6$ g m^{-3}. From Eqs. 10 and 11, it follows that the density and the relative refractive index of particulate matter are related through

$$\rho = 1 + (\Delta\rho/\Delta n)(n - 1) = 1 + 2.22(n - 1) \quad \text{or} \quad (12)$$

$$n = 1 + 0.45(\rho - 1) \quad (12')$$

When such particulate matter, after filtration, is dried before being weighed, only the organic matter remains whose apparent density, ρ_a, corresponds to the quantity $\rho_o V_o$. Note that $V_o = (\rho - 1)/\Delta\rho$.

According to Fig. 5, the quantity $b_p(\lambda)/C_v$ is approximately 0.43×10^6 m^{-1} when n is around 1.05 and the Junge exponent is 4.0. For $n = 1.05$, $V_o = 0.316$ (Eq. 10) and ρ_a is 0.438×10^6 g m^{-3}. Therefore, the mass-specific scattering coefficient is

$$b_p^m(\lambda) = \frac{0.43 \times 10^6 \text{ m}^{-1}}{0.438 \times 10^6 \text{ g m}^{-3}} \approx 1.0 \text{ m}^2 \text{ g}^{-1}$$

Such a value (actually between 0.85 and 1.15 for $j = 3.8$ and 4.2, respectively) is typical of living algal and heterotrophic organisms, to the extent that a 70% water content and a 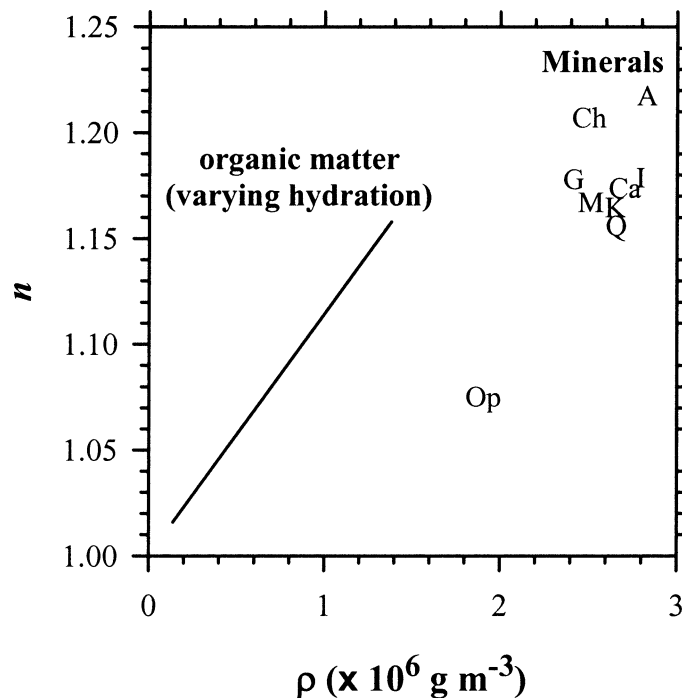relative refractive index around 1.05 are typical for such particles (Aas 1996). One could expect that organic debris (cell walls, broken cytoplasms, etc.) contains less water, so that the question arises of how $b_p^m(\lambda)$ changes with increasing V_o. A diminishing water content entails concomitant increases in n and ρ (Eqs. 10 and 11). With respect to the resulting $b_p^m(\lambda)$ values, these increases compensate each other almost exactly when $j = 4$ (Fig. 6) and $b_p^m(\lambda)$ remains unchanged in spite of the change in water content. This is no longer the case when j differs from four, with variations in $b_p^m(\lambda)$ by $\pm30\%$ at the most. The assumption of perfectly transparent particles can be relaxed to quantify the impact of weak absorption upon scattering. By adopting the n' value of 8×10^{-4} at 555 nm (*see below and Fig. 8*) combined with $n = 1.05$, slightly lower $b_p^m(555)$ values are obtained (Fig. 6).

Mineral particles—There is no tight relationship between the index of refraction and the density for various minerals (*see Fig. 7 and Table 4*). More importantly, for relative indices around 1.18, changes in $b_p(\lambda)/C_v$ are strongly dependent on the Junge exponent (Fig. 5) and predictions are thus less feasible. In contrast to watery organic particulate matter, there is no need to account for a density change due to the presence of water, and therefore $\rho_a = \rho$, at least as a first approximation. A typical example of mineral particles could be that of a population with $j = 4.0$, $n = 1.18$, and $\rho = 2.7 \times 10^6$ g m^{-3}. This leads to $b_p^m(\lambda)/C_v \approx 1.55 \times 10^6$ m^{-1} (Fig.

5), which results in $b_p^m(\lambda) \approx 0.57$ m^2 g^{-1} (or 0.36 and 0.81 m^2 g^{-1} when $j = 3.8$ and 4.2, respectively). If mineral particles contain a certain amount of water (maybe colloidal particles enter into this category) the above values would tend to increase, whereas a slight decrease is expected if minerals are absorbing.

Although inevitable uncertainties remain in the above computations because of unknown lower size limits (and assumptions regarding the size distribution), the qualitative behavior is well described. Specifically, the mass-specific scattering coefficient is distinctly lower for minerogenic particles compared to that of organic particulate assemblages. In natural environments, even in case 1 waters, it is likely that some mineral particles are present (debris and detached liths, or wind-blown terrestrial dust), which results in lowering the $b_p^m(\lambda)$ value with respect to typical values of purely organic material. Conversely, the presence of a significant amount of phytoplankton or other organic material in coastal case 2 waters will result in enhancing $b_p^m(\lambda)$ above the values typical of pure minerogenic suspensions.

Spectral dependency of scattering—If the hypothesis of nonabsorption (approximately justified when $\lambda = 555$ nm) was extended to the whole spectrum, the result would be a scattering spectrum with a shape described by a power law:

$$b_p(\lambda) = B(\lambda/\lambda_0)^{-\gamma} \tag{13}$$

where λ_0 is a reference wavelength, $B = b_p(\lambda_0)$, and the exponent γ is related to the Junge exponent through (Morel 1973):

$$\gamma = j - 3 \tag{13'}$$

Actually, this relationship is strictly true if D_{min} and D_{max} in Eq. 6 are 0 and ∞. It remains approximately true inasmuch as the scattering coefficient is practically insensitive to these limits (*see* discussion by Boss et al. 2001). Introducing absorption, and thus a complex refractive index, generally results in lower scattering. The spectral shape corresponding to Eq. 13 is sensitive to such effects, in particular in the vicinity of the absorption bands where the real part of the refractive index n exhibits weak variations due to anomalous dispersion (e.g., Mueller 1973; Bricaud and Morel 1986).

To quantify such absorption effects, we considered two idealized categories of particulate matter, a purely mineral fraction and a purely algal fraction. The former is given a real part $n = 1.18$ and an imaginary part n' that increases with decreasing wavelength (Fig. 8) in such a way that the resulting spectral absorption conforms to an exponential law:

$$a_{NAP}(\lambda) = a_{NAP}(\lambda_0) \exp\left[-S_{NAP}(\lambda - \lambda_0)\right] \tag{14}$$

where the subscript NAP stands for nonalgal particles and S_{NAP} is a slope with a typical value of 0.012 nm^{-1} as derived from numerous measurements during the COASTℓOOC field campaigns (Babin et al. in press). These n' values are lower than those estimated previously for Saharan dust in the blue spectral domain (Patterson et al. 1977) but higher than those for typical clay minerals (e.g., illite, kaolinite, montmorillonite) determined by Egan and Hilgeman (1979). Various Junge exponents are considered in the computations,
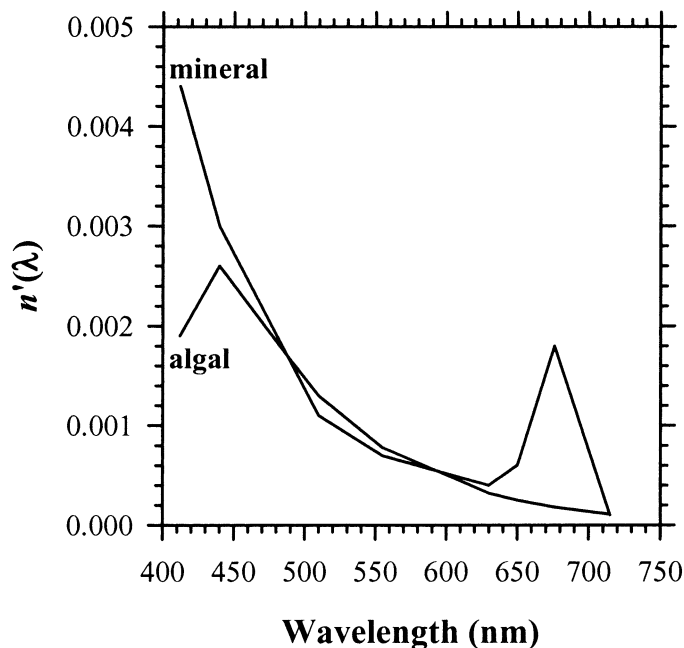

Fig. 8. Typical spectra of the imaginary part of the refractive index for phytoplankton and mineral particles used in our calculations.

and the D_{min} and D_{max} limits are always 0.02 and 200 μm, respectively.

The algal fraction is given the imaginary index varying throughout the spectrum in such a way that a typical absorption spectrum of large phytoplanktonic organisms can be reproduced. This n' spectrum, also shown in Fig. 8, is adopted from Ahn et al. (1992; the data for *Prorocentrum micans* are used as representative of a large algal cell). This n' spectrum is combined with $n = 1.05$. This central n value is then slightly modified by the effect of anomalous dispersion (n varies between 1.04858 and 1.05118). Again various j values are used, and D_{min} is set at 0.45 μm because even the smallest algal pigmented cells are above this size threshold.

Mie theory provides the Q_b and Q_a values at each wavelength for individual particles. Then the weighted sums based on the Junge size distributions are calculated via Eq. 6 to produce the spectral values of the scattering and absorption coefficients for the two kinds of particle populations. Figure 9a shows the spectral scattering coefficients for the mineral and algal populations after normalization by $\langle b_p \rangle$. The corresponding $\varpi_p(\lambda)$ spectra are shown in Fig. 9b. Because of the increasing absorption toward the short wavelengths, the b_p spectra for minerals exhibit a less steep slope than predicted by Eq. 13. For algae, the features (i.e., the troughs) due to pigment absorption are well marked and superposed onto the general slope ruled by the j value.

Observations versus theory

The mass-specific scattering coefficient at 555 nm—The clear difference in the $b_p^m(555)$ values between case 1 and case 2 waters has been previously observed. Baker and Lav-
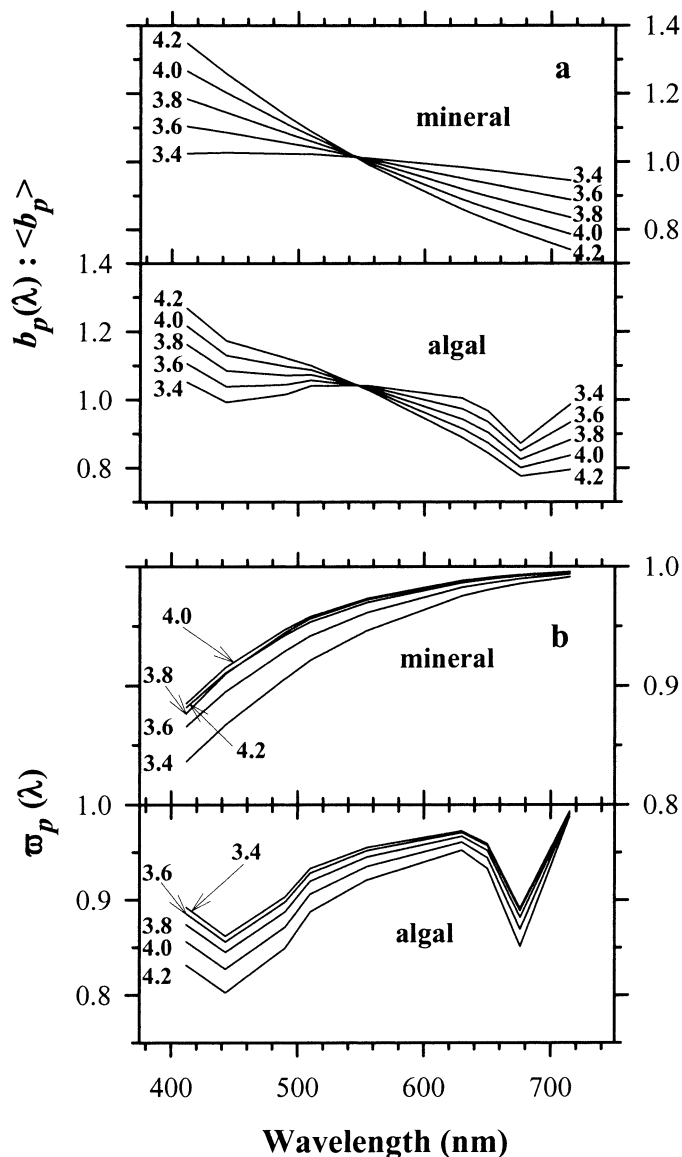
Fig. 9. Computed spectra of (a) the $b_p(\lambda):\langle b_p \rangle$ ratio and (b) the single-scattering albedo $\varpi_p(\lambda)$ for algae and mineral particles (*see text*). Results are shown for different slopes (j) of the Junge-type size distribution.

elle (1984) reported an increase in $b_p^m(555)$ from coastal to open ocean waters. Within the upper layer of various oceanic case 1 waters, Gordon and Morel (1983) found an average $b_p^m(550)$ of 1.0 m² g⁻¹, which is consistent with our observations in the Atlantic samples (Table 4). During a spring bloom in the North Atlantic (Gardner et al. 1993), and in the oligotrophic tropical Pacific (Claustre et al. 1999), the observed carbon-specific beam attenuation coefficients (at 660 nm), $c_p^C(660)$, were 2.6 and 2.0 m² (mg C)⁻¹, respectively. Since the beam attenuation coefficient is very close to the scattering coefficient at 660 nm (it is higher by 3–6% at the most), $c_p^C(660)$ can be transformed into the mass-specific scattering coefficient on the basis of the conversion ratio already used [2.6 g/(g C)]. This calculation leads to $b_p^m(555) = 1.0$ and 0.77 m$^{2(g-1)}$ for the Gardner et al. and

Claustre et al. data, respectively, in agreement with the present results within the accuracy of such estimates (the change in wavelength from 660 to 555 nm does not impact the results in a significant manner).

The average $b_p^m(555)$ value for case 2 waters (0.51 m² g⁻¹) is close to previously published values for coastal and inland waters (Baker and Lavelle 1984 and references therein; Hofmann and Dominik 1995). A considerable variability in $b_p^m(555)$ is, however, observed within each region and on a region-by-region basis. This variability originates from variability in the size distribution (*see Fig. 10*) and from the composition of particulate assemblage, especially the proportion of organic and inorganic particles. The fact that particles can strongly absorb light (e.g., in the Baltic, Fig. 3c) also has a significant role in determining $b_p^m(555)$.

Mie calculations for organic matter for $j = 4$ show that $b_p^m(555)$ is expected to vary only slightly around 1.0 m² g⁻¹ as observed in case 1 waters (Fig. 6). The calculations also show that $b_p^m(555)$ varies around 0.5 m² g⁻¹ for various types of minerals with $3.8 \le j \le 4.0$ (Fig. 10), which is in agreement with our observations in case 2 waters when mineral particles dominate (Tables 2 and 3). For these particles, $b_p^m(555)$ would be first sensitive to the size distribution and then to the refractive index or mineral type. It is worth noting that, as suggested by Fig. 4a, a significant part of the dependency of $b_p^m(555)$ on j results from the contribution to scattering by particles <0.45 μm, which do not contribute to the measured dry weight when using a GF/F glass fiber filter. This problem is much more acute when the measured particle load included only particles with a size >2 μm, as was often the case in previous studies (*see Introduction*). Only ca. 20% of the actual scattering would be related to the >2-μm fraction when particles are mineral (Fig. 4a). This problem of mismatch between methodologies, as well as other methodological issues, especially spatial and temporal mismatch between the in situ measurements of $b_p(\lambda)$ and SPM determinations from discrete water samples, indicates that well-designed sampling strategies are needed in highly variable coastal waters to reduce such experimental errors in the relationships between light scattering and particulate load.

The Baltic Sea is peculiar in the sense that while particles are mostly organic (87%), the average $b_p^m(555)$ value (0.49 m² g⁻¹) is close to the values found in regions dominated by mineral particles (Tables 2 and 3). Absorption is probably the most significant factor that may explain such low $b_p^m(555)$ values. As already noted, especially low $\varpi_p(\lambda)$ values were observed in the Baltic Sea (even at 555 nm), and such an enhanced absorption certainly reduces $b_p^m(555)$. Besides absorption, the only way to reconcile the organic nature of particles with the low $b_p^m(555)$ based on our Mie calculations for nonabsorbing particles (*see Fig. 10*) is to assume that organic particles in the Baltic Sea (1) had a low water content and (2) were on average larger (i.e., lower j value) than in other regions. The first assumption is implied by the fact that phytoplankton represent only a moderate fraction (~50%) of organic matter in the Baltic Sea (Table 3), and therefore this matter might be less hydrated than living cells. For 160 samples collected in the Baltic Sea, Jonasz (1983) found an average j of 3.2 for the size range between 2 and
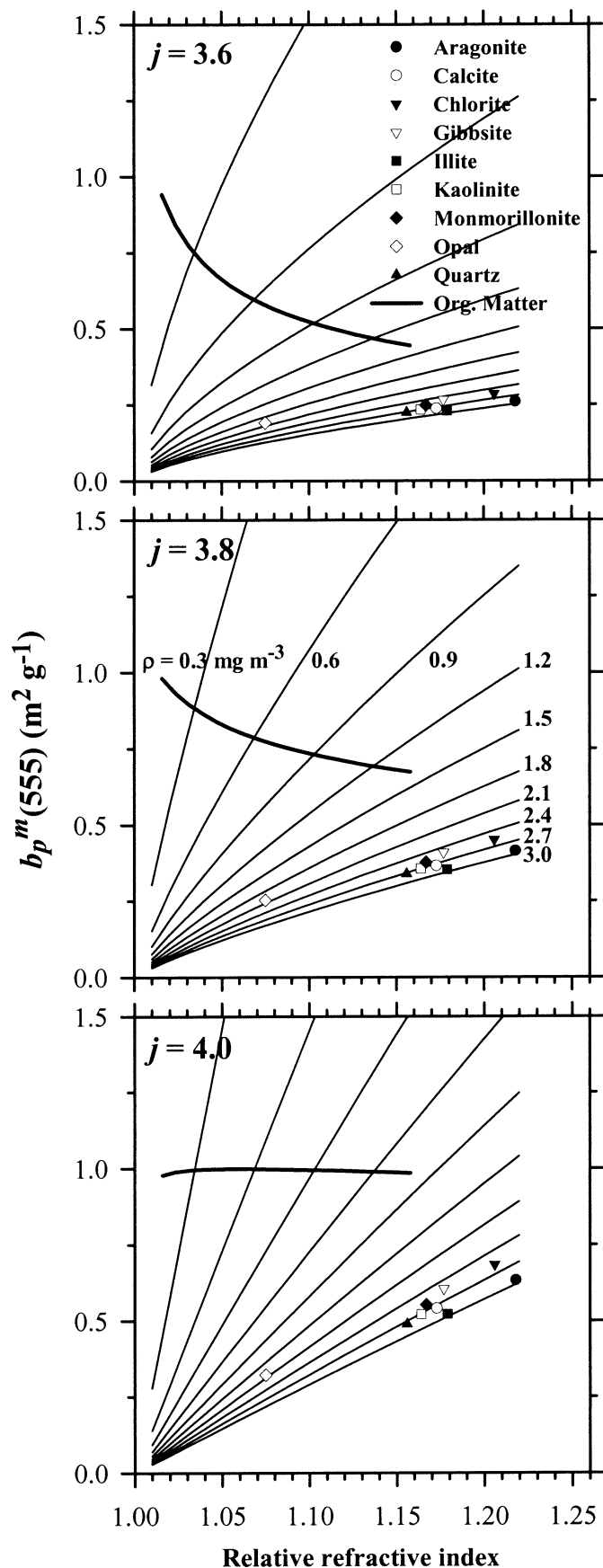
7.5 μm. Compared with other regions, this value seems to be significantly lower (Fig. 10 in Jonasz 1983). Together with the fact that particles below 7.5 μm contribute more than 80% to scattering (Fig. 4a), this supports our second assumption about the lower *j*. Gustafsson et al. (2000) speculated that particle aggregation combined with lower density of organic matter would result in larger sizes of suspended particles in the Baltic Sea.

Spectral variations of the scattering coefficient—As shown in Fig. 3b, the spectral changes in $b_p(\lambda)$ are poorly represented by a λ^{-1} law, often adopted when describing $b_p(\lambda)$ (e.g., Morel 1988; Lee et al. 1994; Garver and Siegel 1997). The λ^{-1} law is only valid for a population of non-absorbing particles following a Junge-type size distribution with *j* = 4 (Eq. 13′). It has been shown by Babin et al. (in press) that the relative contribution of phytoplankton and nonalgal particles to absorption was significant in all case 2 regions during the COASTℓOOC experiments (*see* their Table 7). For our case 1 water samples, the $b_p(\lambda)$: $\langle b_p \rangle$ spectrum is obviously affected by absorption with clear minima within the main phytoplankton pigment absorption bands (Fig. 3a). Such scattering reduction is typical for particle populations dominated by phytoplankton (e.g., Stramski et al. 2001). The simulated algal $b_p(\lambda)$: $\langle b_p \rangle$ spectrum (Figs. 9a and 11a) for *j* = 3.6 nicely reproduces the averaged spectrum for case 1 waters.

The examined case 2 waters, where a phytoplanktonic population coexists with a mineral suspension, cannot be directly compared to hypothetical scattering spectra computed for pure mineral suspensions. However, the averaged $b_p(\lambda)$: $\langle b_p \rangle$ spectrum for case 2 waters is very close to that computed for pure minerals, with a Junge exponent of 3.4, although some prints of algal pigments are apparent (Fig. 11b). If the geographic regions are considered separately (Fig. 3a), specific features of the scattering spectra [also revealed in the $\varpi_p(\lambda)$ spectra in Fig. 3c] can be explained. The $\varpi_p(\lambda)$ spectra for the Baltic and the North Sea exhibit a drop in the blue, which is compatible with the absorption budget presented in Babin et al. (in press) and with the observation of high yellow substance content, probably partly associated with the particles.

The average $b_p(\lambda)$: $\langle b_p \rangle$ spectra found by Barnard et al. (1998) and Gould et al. (1999) were slightly different from the ones reported here. While Barnard et al. data seem to be representative of phytoplankton-dominated waters, the steep increase in Gould et al. data toward the blue suggests that mineral particles dominated their samples (Fig. 3b).

It is worth noting that our observations of small spectral variations in $b_p(\lambda)$, together with the absence of particulate

←

Fig. 10. Theoretical relationship between the mass-specific scattering coefficient and the relative index of refraction for different values of ρ (the different curves) and different values of *j* (the different panels). The position of various mineral species is also shown for the *n* and ρ values given in Table 6. The bold solid line illustrates the relationship for organic matter associated with various amounts of water (*see* text and Fig. 6).
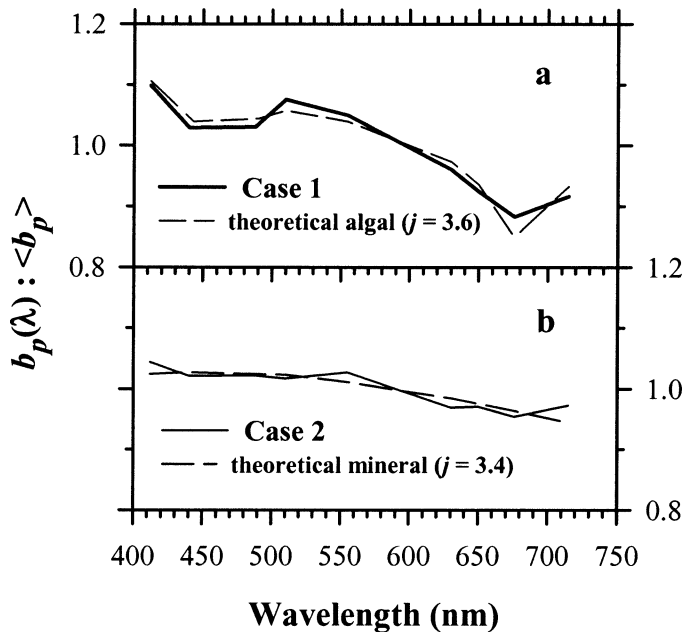
Wavelength (nm)

Fig. 11. The observed average spectra of the $b_p(\lambda):\langle b_p\rangle$ ratio for (a) case 1 and (b) case 2 waters (*see also Fig. 3*). The calculated spectra for typical pure phytoplankton and pure mineral particles are also shown.

absorption in the near-infrared (Babin and Stramski 2002), support the simple correction approach used here and in the past for eliminating the scattering error from absorption measurements made with the reflective-tube technique, that is, the subtraction of the absorption signal at 715 nm from the signal measured at all other wavelengths. As the $b_p(555):a(440)$ ratio is on average around three, the remaining error in the determination of the absorption coefficient due to scattering is expected to have a minor impact on the determination of the scattering coefficient.

We collected a significant amount of data on the spectral scattering coefficient of particles, $b_p(\lambda)$, and mass concentration of suspended particulate matter, SPM, in various coastal marine environments around Europe and some open ocean waters. The overall range of b_p and SPM in these data spans over three orders of magnitude, and the data reveal variations among regions and within regions in the $b_p(\lambda)$ versus SPM relationship, and thus in the mass-specific scattering coefficient, $b_p^m(\lambda)$. This coefficient exhibits markedly differing values in coastal waters (case 2) and in open ocean Atlantic waters (case 1). In coastal waters, the average values of $b_p^m(555)$ are close to 0.5 m^2 g^{-1}, with relatively little variation among the various regions. In the Atlantic case 1 waters, this coefficient is about 1.0 m^2 g^{-1}. The primary cause for this difference is the increased role of nonwatery inorganic particles in coastal waters, compared to open ocean waters typically dominated by organic particles. All our measurements consistently showed that for the waters studied the general spectral slope of the scattering coefficient is less steep than that described by a λ^{-1} dependency, which was often adopted for open ocean oligotrophic waters. This likely results from the effects of increased absorption toward the blue spectral domain, which is characteristic for most marine

particles in the coastal environments studied here (Babin et al. in press), or from a relatively small slope of the particle size distribution, or both.

Although significant variability in scattering properties was observed, these results will allow simple parameterizations of scattering by seawater particles, in support of different applications such as in situ and optical remote sensing of particle load. To make further progress in these applications, we need to improve our knowledge of the particle scattering phase function, since it is still limited to relatively few determinations (e.g., Petzold 1972; Morel 1973; Kullenberg 1974, 1984).

References

AAS, E. 1981. The refractive index of phytoplankton, p. 61. Department of Geophysics, Univ. Oslo.
———. 1996. Refractive index of phytoplankton derived from its metabolite composition. J. Plankton Res. **18:** 2223–2249.
AHN, Y.-H., A. BRICAUD, AND A. MOREL. 1992. Light backscattering efficiency and related properties of some phytoplankters. Deep-Sea Res. **39:** 1835–1855.
BABIN, M., AND D. STRAMSKI. 2002. Light absorption by aquatic particles in the near-infrared spectral region. Limnol. Oceanogr. **47:** 911–915.
———, AND OTHERS. In press. Variations in the light absorption coefficients of phytoplankton, non-algal particles, and dissolved organic matter in coastal waters around Europe. J. Geophys. Res.
BADER, H. 1970. The hyperbolic distribution of particle sizes. J. Geophys. Res. **75:** 2822–2830.
BAKER, E. T. 1976. Distribution, composition, and transport of suspended particulate matter in the vicinity of Willapa submarine canyon, Washington. Geol. Soc. Am. Bull. **87:** 625–632.
———, G. A. CANNON, AND H. C. CURL, JR. 1983. Particle transport processes in a small marine bay. J. Geophys. Res. **88:** 9661–9669.
———, AND J. W. LAVELLE. 1984. The effect of particles size on the light attenuation coefficient of natural suspensions. J. Geophys. Res. **89:** 8197–8203.
———, D. A. TENNANT, R. A. FEELY, G. T. LEBON, AND S. L. WALKER. 2001. Field and laboratory studies on the effect of particle size and composition on optical backscattering measurements in hydrothermal plumes. Deep-Sea Res. I **48:** 593–604.
BARNARD, A. H., W. S. PEGAU, AND J. R. V. ZANEVELD. 1998. Global relationships of the inherent optical properties of the oceans. J. Geophys. Res. **103:** 24955–24968.
BEARDSLEY, J., F. GEORGE, H. PAK, AND K. L. CARDER. 1970. Light scattering and suspended particles in the Eastern Equatorial Pacific Ocean. J. Geophys. Res. **75:** 2837–2845.
BOSS, E., M. S. TWARDOWSKI, AND S. HERRING. 2001. Shape of the particulate beam attenuation spectrum and its inversion to obtain the shape of the particulate size distribution. Appl. Opt. **40:** 4885–4893.
BRICAUD, A., AND A. MOREL. 1986. Light attenuation and scattering by phytoplanktonic cells: A theoretical modeling. Appl. Opt. **25:** 571–580.
CARDER, K. L., J. BEARDSLEY, F. GEORGE, AND H. PAK. 1971. Particle size distribution in the Eastern Equatorial Pacific. J. Geophys. Res. **76:** 5070–5077.
———, P. R. BETZER, AND D. W. EGGIMANN. 1975. Physical, chemical and optical measures of suspended-particle concentrations: Their intercomparison and application to the West African

Shelf, p. 173–193. *In* J. Gibbs [ed.], Suspended solids in water. Plenum.

———, AND F. C. SCHLEMMER II. 1973. Distribution of particles in the surface waters of the Eastern Gulf of Mexico: An indicator of circulation. J. Geophys. Res. **78:** 6286–6299.

CHAVEZ, F. P. AND OTHERS. 1995. On the chlorophyll-a retention properties of glass-fiber GF/F filters. Limnol. Oceanogr. **40:** 428–433.

CLAUSTRE, H., AND OTHERS. 1999. Variability in particle attenuation and stimulated fluorescence in the tropical and equatorial Pacific: Scales, patterns and some biogeochemical implications. J. Geophys. Res. **104:** 3401–3422.

———, AND OTHERS. 2000. Continuous monitoring of surface optical properties across a geostrophic front: Biogeochemical inferences. Limnol. Oceanogr. **45:** 309–321.

COPIN-MONTÉGUT, G. 1980. Matière en suspension dans les eaux de mer: répartition, composition chimique, origine et évolution, p. 173, Laboratoire de Physique et Chimie Marines. Thesis, Université Pierre et Marie Curie.

EGAN, W. G., AND T. W. HILGEMAN. 1979. Optical properties of inhomogeneous materials: Applications to geology, astronomy, chemistry, and engineering. Academic.

EGGIMANN, D. W., P. R. BETZER, AND K. L. CARDER. 1980. Particle transport from the West African shelves of Liberia and Sierra Leone to the deep sea: A chemical approach. Mar. Chem. **9:** 283–306.

FERRARI, G. M., F. G. BO, AND M. BABIN. In press. Geo-chemical and optical characterization of suspended matter in European coastal waters. Estuar. Coast. Shelf Sci.

GARDNER, W. D., I. D. WALSH, AND M. J. RICHARDSON. 1993. Biophysical forcing of particle production and distribution during a spring bloom in the North Atlantic. Deep-Sea Res. II **42:** 757–775.

GARVER, S. A., AND D. A. SIEGEL. 1997. Inherent optical properties inversion of ocean color spectra and its biogeochemical interpretation 1. Time series from the Sargasso Sea. J. Geophys. Res. **102:** 18607–18625.

GORDON, H. R., AND A. MOREL. 1983. Remote assessment of ocean color for interpretation of satellite visible imagery. Springer.

GOULD, R. W., R. A. ARNONE, AND P. M. MARTINOLICH. 1999. Spectral dependence of the scattering coefficient in case 1 and case waters. Appl. Opt. **38:** 2377–2383.

GUSTAFSSON, Ö., A. WIDERLUND, P. S. ANDERSSON, J. INDRI, P. ROOS, AND A. LEDIN. 2000. Colloid dynamics and transport of major elements through a boreal river—brackish bay mixing zone. Mar. Chem. **71:** 1–21.

HOFMANN, A., AND J. DOMINIK. 1995. Turbidity and mass concentration of suspended matter in lake water: A comparison of two calibration methods. Aquat. Sci. **57:** 54–69.

HUNKINS, K., E. M. THORNDIKE, AND G. MATHIEU. 1969. Nepheloid layers and bottom currents in the Arctic Ocean. J. Geophys. Res. **74:** 6995–7008.

JERLOV, N. G. 1955. The particulate matter in the sea as determined by means of the Tyndall meter. Tellus **7:** 218–225.

JONASZ, M. 1983. Particle-size distribution in the Baltic. Tellus **35B:** 346–358.

KIRK, J. T. O. 1994. Light and photosynthesis in aquatic ecosystems, 2nd ed. Cambridge Univ. Press.

KITCHEN, J. C., O. C. ZAFIRIOU, AND H. PAK. 1978. The vertical structure and size distributions of suspended particles off Oregon during the upwelling season. Deep-Sea Res. **25:** 453–468.

KULLENBERG, G. 1974. Observed and computed scattering functions, p. 25–49. *In* N. G. Jerlov and E. Steemann-Nielsen [eds.], Optical aspects of oceanography. Academic.

———. 1984. Observations of light scattering functions in two oceanic areas. Deep-Sea Res. **31:** 295–316.

LEE, Z., K. L. CARDER, S. K. HAWES, R. G. STEWARD, T. G. PEACOK, AND C. O. DAVIS. 1994. Model interpretation of hyperspectral remote-sensing reflectance. Appl. Opt. **33:** 5721–5732.

LIDE, D. R. 2001. CRC handbook of physics and chemistry, 82 ed. CRC.

MCCAVE, I. N. 1983. Particulate size spectra, behavior, and origin of nepheloid layers over the Nova Scotia continental rise. J. Geophys. Res. **88:** 7647–7666.

MOREL, A. 1973. Diffusion de la lumière par les eaux de mer. Résultats expérimentaux et approche théorique, p. 3.1-1-71, Optics of the sea. AGARD Lectures Series.

———. 1988. Optical modeling of the upper ocean in relation to its biogenous matter content (Case I waters). J. Geophys. Res. **93:** 10749–10768.

———, AND Y.-H. AHN. 1990. Optical efficiency factors of free-living marine bacteria: Influence of bacterioplankton upon the optical properties and particulate organic carbon in oceanic waters. J. Mar. Res. **48:** 145–175.

———, AND ———. 1991. Optics of heterotrophic nanoflagellates and ciliates: A tentative assessment of their scattering role in oceanic waters compared to those of bacterial and algal cells. J. Mar. Res. **49:** 177–202.

———, AND S. MARITORENA. 2001. Bio-optical properties of oceanic waters: A reappraisal. J. Geophys. Res. **100:** 7163–7180.

———, AND L. PRIEUR. 1977. Analysis of variations in ocean color. Limnol. Oceanogr. **22:** 709–722.

MUELLER, J. L. 1973. The influence of phytoplankton on ocean color spectra. Ph.D. Thesis, Oregon State University.

OWEN, W. O., JR. 1974. Optically effective area of particle ensembles in the sea. Limnol. Oceanogr. **19:** 584–590.

PAK, H., J. BEARDSLEY, F. GEORGE, G. R. HEATH, AND H. CURL. 1970*a.* Light-scattering vectors of some marine particles. Limnol. Oceanogr. **15:** 683–687.

———, ———, ———, AND P. K. PARK. 1970*b.* The Columbia River as a source of marine light-scattering particles. J. Geophys. Res. **75:** 4570–4578.

———, AND J. R. V. ZANEVELD. 1977. Bottom nepheloid layers and bottom mixed layers observed on the continental shelf off Oregon. J. Geophys. Res. **82:** 3921–3931.

———, ———, J. BEARDSLEY, AND F. GEORGE. 1971. Mie scattering by suspended particles. J. Geophys. Res. **76:** 5065–5069.

PATTERSON, E. M., D. A. GILLETTE, AND B. H. STOCKTON. 1977. Complex index of refraction between 300 and 700 nm for Saharan aerosols. J. Geophys. Res. **82:** 3153–3160.

PEGAU W. S., G. DERIC, AND J. R. V. ZANEVELD. 1997. Absorption and attenuation of visible and near-infrared light in water: Dependence on temperature and salinity. Appl. Opt. **36:** 6035–6046.

———, AND OTHERS. 1995. A comparison of methods for the measurement of the absorption-coefficient in natural waters. J. Geophys. Res. **100:** 13201–13220.

PETZOLD, T. J. 1972. Volume scattering functions for selected ocean water, p. 79. Scripps Institution of Oceanography.

PICKARD, G. L., AND L. F. GIOVANDO. 1960. Some observations of turbidity in British Columbia inlets. Limnol. Oceanogr. **5:** 162–170.

SATHYENDRANATH, S., L. PRIEUR, AND A. MOREL. 1989. A three-component model of ocean colour and its application to remote sensing of phytoplankton pigments in coastal waters. Int. J. Remote Sens. **10:** 1373–1394.

SHELDON, R. W. 1972. Size separation of marine seston by membrane and glass-fiber filters. Limnol. Oceanogr. **17:** 494–498.

———, A. PRAKASH, AND W. H. J. SUTCLIFFE. 1972. The size dis-

tribution of particles in the ocean. Limnol. Oceanogr. **17:** 327–340.

SPINRAD, R. W. 1986. A calibration diagram of specific beam attenuation. J. Geophys. Res. **91:** 7761–7764.

———, AND J. R. V. ZANEVELD. 1982. An analysis of the optical features of the near-bottom and bottom nepheloid layers in the area of the Scotian rise. J. Geophys. Res. **87:** 9553–9561.

———, ———, AND J. C. KITCHEN. 1983. A study of the optical characteristics of the suspended particles in the benthic nepheloid layer of the Scotian Rise. J. Geophys. Res. **88:** 7641–7645.

STRAMSKI, D. 1990. Artifacts in measuring absorption spectra of phytoplankton collected on a filter. Limnol. Oceanogr. **35:** 1804–1809.

———, A. BRICAUD, AND A. MOREL. 2001. Modeling the inherent optical properties of the ocean based on the detailed composition of planktonic community. Appl. Opt. **40:** 2929–2945.

———, AND D. A. KIEFER. 1991. Light scattering by microorganisms in the open ocean. Prog. Oceanogr. **28:** 343–383.

TASSAN, S., AND G. M. FERRARI. 1995. An alternative approach to absorption measurements of aquatic particles retained on filters. Limnol. Oceanogr. **40:** 1358–1368.

TSUDA, R., AND K. NAKATA. 1982. Particle size distribution and light scattering in Akita Bay. La Mer **20:** 1–8.

VAN DE HULST, H. C. 1957. Light scattering by small particles, John Wiley.

VAN DER LINDE, D. W. 1998. Protocol for determination of total suspended matter in oceans and coastal zones. JRC Technical Note I.98.182.

VAN RAAPHORST, W., AND J. F. P. MALSCHAERT. 1996. Ammonium adsorption in superficial North Sea sediments. Cont. Shelf Res. **16:** 1415–1435.

VIDUSSI, F., H. CLAUSTRE, J. BUSTILLOS-GUZMAN, C. CAILLAU, AND J.-C. MARTY. 1996. Rapid HPLC method for determination of phytoplankton chemotaxinomic pigments: Separation of chlorophyll a from divinyl-chlorophyll *a,* and zeaxanthin from lutein. J. Plankton Res. **18:** 2377–2382.

ZANEVELD, J. R. V., J. C. KITCHEN, AND C. MOORE. 1994. The scattering error correction of reflecting-tube absorption meters, p. 44–55, Ocean Optics XII. Soc. Photo-Optical Instrum. Eng. (SPIE).

———, AND H. PAK. 1979. Optical and particulate properties at oceanic fronts. J. Geophys. Res. **84:** 7781–7790.